Larhyss Journal, ISSN 1112-3680, n°59, Sept 2024, pp.29-51

REMOVAL OF AZO TOXIC DYE FROM AQUEOUS SOLUTIONS USING DRY SPEARMINT SPRIGS

***BOUDAOUD A.*[1*], *AD C.*[2], *DJEDID M.*[2], *GUERMIT M.*[1], *BENALIA M.*[2], *SOLTANI A.*[3]**

[1]Amar Telidji University of Laghouat, Faculty of Technology, Department of The Common Trunk Sciences and Technology, P.O. Box 37G, Ghardaia Road, 03000 Laghouat, Algeria
[2]Amar Telidji University of Laghouat, Faculty of Technology, Department of Process Engineering, P.O. Box 37G, Ghardaia Road, 03000 Laghouat, Algeria
[3] Higher Normal School of Laghouat, Trans-Saharan Hwy 04033 Laghouat, Algeria

(*) a.boudaoud@lagh-univ.dz

Research Article – Available at http://larhyss.net/ojs/index.php/larhyss/index
Received April 16, 2024, Received in revised form August 22, 2024, Accepted September 1, 2024

ABSTRACT

The main objective of this study was to investigate the mechanism of methyl violet 10B dye adsorption onto dry sprigs of Spearmint, determine the most suitable kinetic and isothermal models for the adsorption process, and estimate the maximum adsorption capacity for the dye. The experimental results revealed that the optimal adsorption conditions were achieved with an adsorbent mass of 0.01 grams, a pH of 5, and an equilibration time of 30 minutes. The adsorption capacity of the methyl violet 10B dye increased with increasing initial dye concentration but decreased as the temperature increased. The pseudo-second-order kinetic model provided the best fit to the experimental data. The Temkin isotherm model demonstrated the best fit, and the maximum adsorption capacity for monolayer adsorption was 84.83 mg/g. The thermodynamic parameters confirmed that the adsorption process was spontaneous ($\Delta G°<0$), exothermic ($\Delta H°<0$), and random ($\Delta S°<0$). The adsorbent exhibited promising results, including high removal efficiency of methyl violet 10B, low cost, and environmental friendliness. These findings suggest that the adsorbent has the potential to serve as a viable alternative for sustainable wastewater treatment.

Keywords: Methyl violet 10B dye, Sustainable Adsorbent, Dry Spearmint Sprigs, Kinetics, Isotherm, Thermodynamics.

INTRODUCTION

Water pollution from synthetic dyes is a significant environmental concern due to its potential adverse impacts on human health and aquatic ecosystems. The global production of synthetic dyes has risen over the years, while the consumption of dyeing auxiliary chemicals and water consumption in the finishing sector have increased significantly (Berradi et al., 2019; Benslama et al., 2021). These dyes have wide applications in various industries. Although dyes enhance the appearance of products, many concerns about toxins have been raised (Al-Tohamy et al., 2022).

The textile industry in Algeria significantly contributes to water pollution through the use of dyes. The Oued D'Hous River in Algeria, for example, is heavily polluted by domestic, industrial, and agricultural wastewater, which includes dyes from the textile industry (Samai et al., 2023). In Tlemcen (Algeria) also faces similar pollution issues due to the discharge of untreated wastewater containing textile dyes (Djehaf et al., 2019). Effluents from dyes usually have a high biological and chemical oxygen demand (BOD and COD) and are very rich in organic and inorganic pollutants, in addition to their discoloration (Benslama et al., 2021).

Among synthetic dyes, azo dyes, anthraquinone dyes, phthalocyanine dyes, and triphenylmethane dyes are widely used and pose specific challenges due to their persistence and potential toxicity (John et al., 2022; Ren et al., 2006).

Methyl violet 10B or crystal violet is a synthetic dye that belongs to the triarylmethane dye family. Crystal violet is sparingly soluble in water, forms a blue–violet solution when dissolved in an aqueous medium, and tends to precipitate at higher concentrations (Ouettar et al., 2023; Castellar-ortega et al., 2022). It is used in various industries, such as textiles, inks, paints and printing materials, as a colorant and as a biological stain to study bacteria under microscopes (Adak et al., 2005).

The toxicity of methyl Violet 10B depends on different factors, such as the exposure duration, exposure route and sensitivity of exposed organisms. The maximum concentration of methyl violet 10B that can be considered toxic in water varies across different organisms and environmental conditions (Mani and Bharagava, 2016). However, it is generally recognized that elevated concentrations of methyl violet 10B can have toxic effects on aquatic organisms, particularly fish and invertebrates. At these concentrations, methyl violet 10B can impair plant growth, reproduction, and overall physiological functions, ultimately leading to disruptions in the ecosystem (Kyi et al., 2020).

Crystal violet is not easily biodegradable, meaning it can persist in the environment for extended periods. This persistence can result in bioaccumulation in organisms and potential biomagnification through the food chain (Rehman et al., 2017).

Methyl violet 10B has been associated with potential health risks, especially with prolonged or excessive exposure. It has been shown to have cytotoxic effects on mammalian cells (Pnninks et al., 2017), and studies have indicated the genotoxic and mutagenic properties of crystal violet and its breakdown products. Furthermore, Crystal

Violet has been classified as a possible human carcinogen by some regulatory agencies (Sun et al., 2019; Docampo and Moreno, 2001).

To address these environmental and health concerns, there is an urgent need to develop eco-friendly and cost-effective treatment methods for removing dyes from wastewaters (Adesanmi et al., 2022; Loulidi et al., 2020).

Algeria is making great efforts in water conservation by promoting measures to reduce precious resource waste. The country has implemented a policy focused on collecting, treating, and reusing domestic and industrial wastewater (Aroua-berkat and Aroua, 2022). To achieve this, Algeria has 200 wastewater treatment plants that utilize multi-stage treatment processes for effective purification (MRE, 2022). While studies show promising results for adsorption as an alternative water treatment method (Benslama et al., 2021; Khelifi et al., 2018), its application remains limited, often relying on activated carbon despite its high cost (Messaoud-Boureghda et al., 2013).

Moreover, the search for natural and sustainable adsorbents, such as raw lignocellulosic materials or agricultural wastes, is gaining momentum. These adsorbents offer potential solutions for effective dye removal while being environmentally friendly and readily available (Imran et al., 2022; Rezazadeh et al., 2021).

Spearmint is one of the most abundant plants in Algeria, making it a cost-effective and environmentally friendly option. Furthermore, mint it is a valuable resource in alternative medicine. Its use as an adsorbent in wastewater treatment not only provides economic benefits by reducing the cost of treatment but also offers potential health benefits (Belhouala and Benarba, 2021; Hamza et al., 2022)

In this context, our research presents a comprehensive study on the adsorption process of methyl violet 10B (MV10B) dye onto Dry Spearmint Sprigs (DSS), investigates the influence of various factors on this adsorption process, and explores the adsorption mechanism through isotherms, kinetics, and thermodynamic properties.

MATERIAL AND METHODS

Material

Dry Spearmint Sprigs (*Mentha spicata L.*) collected in the area of Laghouat, Algeria, crystal violet or methyl violet 10B ($C_{25}H_{30}N_3Cl$, 99 %), sodium hydroxide (NaOH, 98 %), and sulfuric acid (H_2SO_4, 95 %) were acquired from Sigma–Aldrich (Germany) and used as the materials and reagents in this study.

Preparation of MV10B dye

Methyl violet 10B is a synthetic dye. Its chemical name is Gentian violet or crystal violet (Mahmood and Mahmood, 2023). The chemical structure of crystal violet belongs to the family of triarylmethane dyes. It comprises a central carbon atom (methyl group) connected to three aromatic phenyl rings, each replaced with various functional groups

and methyl groups (Fig. 1). The molecular formula of methyl violet 10B is $C_{25}H_{30}N_3Cl$, and it has a molecular weight of approximately 407.98 g/mol (AL-Shammari and AL-Mammar, 2022).

An MV10B dye solution with a concentration of 1000 mg/L was prepared by dissolving 1.00 g of dye in 1.00 L of distilled water. The remaining concentrations were prepared by diluting this stock solution with distilled water (Srinivas et al., 2023).

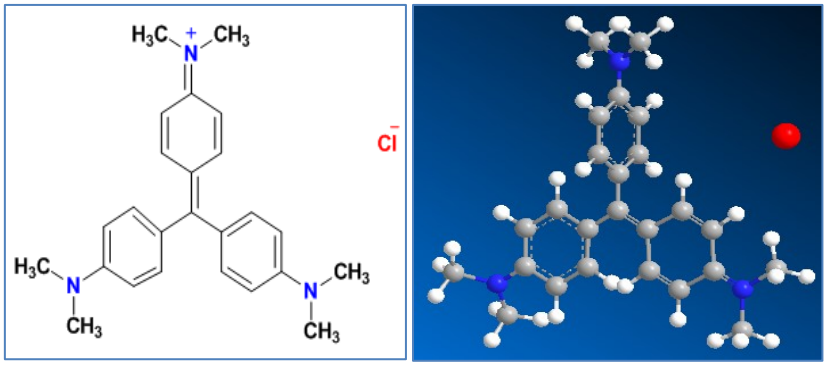

Figure 1: Chemical structure of the dye methyl violet 10B (AL-Shammari and AL-Mammar, 2022)

Preparation of DSS adsorbent

The DSS adsorbent was prepared following the following steps: First, it was washed multiple times with tap water and subsequently with distilled water under boiling conditions to eliminate any impurities. Afterwards, the adsorbent was cut into smaller pieces and dried in an oven at 105 °C. Once the sample had dried, it was crushed and sifted to obtain powder particles with a size smaller than 0.6 mm.

Adsorbent characterization

Fourier transform infrared spectroscopy (FTIR) was used to identify the different bonds and to determine the main functions of the adsorbent. The analysis was carried out on a sample of the DSS adsorbent in the solid state, which formed 2 mg of mass particles. A JASCO FT/IR-4200 FTIR spectrometer was used in this analysis.

Adsorption experiment

Using the batch adsorption experimental setup (Khelili et al., 2024), a set of experiments was carried out to study the different steps of the adsorption process. In glass flasks with a capacity of 250 ml, 100 ml of MV10B dye aqueous solution with an optimal mass of the DSS adsorbent was mixed under optimal conditions. These conditions were determined by sequentially modifying certain parameters associated with the elements of the adsorption process, namely, the adsorbate (MV10B dye), the adsorbent (DSS), and

operational parameters such as the DSS adsorbent mass (0.01-0.8 g), the pH of the solution (2-10), the contact time (0-180 min), the initial concentration of the MV10B dye (15-100 mg/L), and the temperature (293-323 K). The experiments were repeated twice to ensure accuracy of the results. After each experiment, the dye adsorbate was separated from the adsorbent through filtration using a double-boxing ring 102 filter. The residual concentration was measured.

UV spectroscopy was used to measure the dye concentrations before and after the adsorption experiments at 590 nm.

The adsorption efficiency was calculated either in terms of quantity (q (mg/g)) or adsorption rate (R %) using equations (1) and (2):

$$q = \frac{(C_0 - C_e)}{m} \times V \quad (1)$$

$$R\% = \frac{(C_0 - C_e)}{C_0} \times 100 \quad (2)$$

Where C_0 and C_e (mg/L) are the initial and equilibrium concentrations of the MV10B dye, respectively, V (L) is the initial volume of the MV10B dye solution, and m (g) is the weight of the MNS adsorbent.

The Data Analysis and Graphing Software OriginLab 2019 was used to draw all curves and calculate all parameters of the nonlinear models used in the kinetic and isotherm studies of MV10B dye adsorption, including the statistical metrics: the coefficient of determination (R^2), adjusted R^2 (Adj R^2), and chi-squared (χ^2).

RESULTS AND DISCUSSION

FTIR analysis

The FTIR spectrum of the adsorbent displays several characteristic peaks that provide insight into its chemical composition and functional groups (Fig. 2). The broad peaks at 3483 cm^{-1} and 3411 cm^{-1} correspond to O-H stretching vibrations from hydroxyl groups in lignin, cellulose and hemicellulose (Petkova et al., 2019). Their broad shape reveals extensive hydrogen bonding. Additional peaks at 2930 and 2846 cm^{-1} represent C-H stretching in aliphatic structures from lignin and extractives. The presence of carbon dioxide (CO_2) was suggested by the peaks at 2358 and 2331 cm^{-1}, which could be attributed to contamination or molecular interactions involving CO_2. A peak at 1764 cm^{-1} indicates the presence of unconjugated carbonyl groups from ketones, aldehydes and acids related to lignin, pectin, and hemicelluloses (Loulidi et al., 2020). The peak at 1632 cm^{-1} is attributed to conjugated carbonyl groups, which are typical of degraded lignin polymers. The peak at 1392 cm^{-1} confirms aliphatic C-H bending, while the peak at 1247 cm^{-1} is related to C-O stretching in the ether linkages of lignin, cellulose and hemicellulose. Peaks at 1115 and 1043 cm^{-1} correspond to C-O and C-C stretching in cellulose and hemicellulose, respectively. Finally, a peak at 610 cm^{-1} reveals aromatic C-

H bending in lignin structures (Pandey and Pitman, 2003). The FTIR spectrum contains peaks as shown and interpreted in Table 1. These distinct peaks confirm the presence of the main lignocellulosic components, including lignin, cellulose, and hemicellulose molecules, along with their corresponding functional groups, including hydroxyls, aromatic structures (Adapa et al., 2011), and a variety of oxygen-containing groups. This composition is typical for lignocellulosic biomass (Deng et al., 2019).

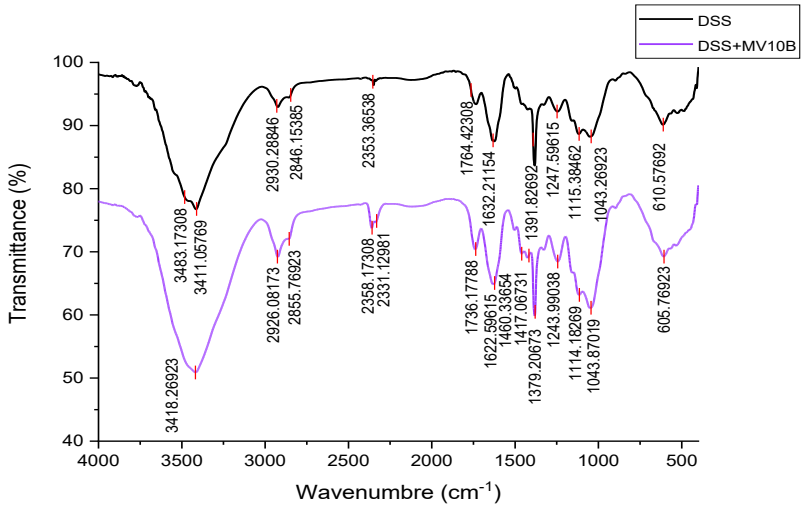

Figure 2: Fourier transform infrared spectra of the DSS and DSS+MV10B dye samples.

Table 1: Functional group assignments of the IR spectra of the DSS and DSS+MV10B dye samples

Wavenumber [cm^{-1}]		Assignement		
SMSL	DSS+ MV10B	Bonds	Functional groups	Biomolecule
3418.27-	3483.17 3411.06	O–H, N–H stretching	Hydroxyl and/or amine	Lignin, cellulose, hemicellulose
2926.08 2855.77	2930.29 2846.15	C–H stretching C–H stretching	Aliphatic and/or aromatic	Lignin, extractives
2358.17 2331.13	2353.37 --	C–O asymmetric stretching vibration	CO_2	Contaminant/ molecular interaction
1736.18 1622.60	1764.42 1632.21	C=O stretching vibration	Carbonyl Aromatic	Lignin, hemicellulose Degraded lignin
1460.34 1417.07	-- --	C–H deformation C–H deformation	Aliphatic and/or aromatic	Lignin, cellulose, hemicellulose

1379.21 1243.99	1391.83 1247.60	C–H deformations C–O stretching	Deformations aryl ethers	Lignin, cellulose, hemicellulose
1114.18 1043.87	1115.38 1043.27	C–O–C stretching C–O, and C–C stretching	Methoxy or ethers Polysaccharides	Cellulose, hemicellulose
605.77	610.58	C-O stretching	Polysaccharides	Lignin

After MV10B dye adsorption (Fig. 2), the intensity of all the peaks increased, indicating potential interactions between the MV10B dye and the functional groups of the adsorbent (Priyantha et al., 2021). The presence of hydroxyl groups (O-H) suggested hydrogen bonding interactions between the dye and the material. The retention of aliphatic components and methyl and methylene groups indicated that these structural elements remained intact even after dye adsorption. The presence of carbonyl groups and unsaturated carbonyl compounds suggested the retention of carbonyl-containing compounds in the material. Peaks corresponding to ether linkages, polysaccharides, and aromatic structures were also observed, indicating that these components were still present even after MV10B dye adsorption. These results suggest that the dye adsorption process did not significantly alter the overall composition of the lignocellulose material. The increased intensity of the peaks after adsorption implies the involvement of functional groups in the adsorption mechanism (El Naeem et al., 2022).

Influential factors on dye adsorption

Understanding the factors that influence the adsorption process is crucial for optimizing adsorption processes and enhancing their performance (Khelifi et al., 2016; Ouakouak and Youcef, 2016). These factors include the mass of the adsorbent, the initial concentration the contact time, the pH, and the temperature. By controlling these factors, it is possible to enhance the adsorption capacity and efficiency of the adsorption process (Abba et al., 2019; Chauhan and Dikshit, 2023). Increasing the adsorbent mass can enhance adsorption due to the greater surface area available. Contact time is also important, as the adsorption process reaches equilibrium and becomes constant over time (Chauhan and Dikshit, 2023). The pH of the solution can influence the surface charge and ionization of the adsorbent and adsorbate, leading to a higher affinity between them (Yeddou Mezenner et al., 2012). Temperature can affect the solubility and diffusion rate of the adsorbate molecules, enhancing the adsorption process (Youcef et al., 2014).

In this section, the effect of various factors on dye adsorption is studied, and the optimal values for these factors are determined to achieve the highest possible efficiency of the adsorbent (Fig. 3).

Effect of adsorbent mass

Fig. 3a illustrates the impact of varying masses of the DSS adsorbent on dye adsorption. The point of intersection between the adsorption amount (q) and efficiency ratio (R %) values indicates that the optimal dose for this adsorption process is 0.1 g of the DSS

adsorbent. Beyond this specified mass, any increase in the adsorbent mass did not further increase its adsorption efficiency.

Effect of pH

Investigating the influence of pH on adsorption performance is essential for optimizing and engineering effective adsorption systems for dye removal from wastewater (Soltani et al., 2021).

The effect of pH on the adsorption of cationic dye is shown in Fig. 3b. The maximum adsorption efficiency is achieved at a pH of 5, after which the adsorption constant. This indicates that in acidic media (pH< 5), the adsorbent material tends to exhibit a negatively charged surface due to the dissociation of functional groups present on its surface, such as carboxyl or hydroxyl groups. This negative surface charge enables favorable electrostatic interactions with the cationic dye, leading to increased adsorption efficiency (Kant et al., 2014).

Furthermore, the wide pH range (pH > 5) over which adsorption occurs suggests the robustness of the adsorbent material in maintaining its negative charge and facilitating dye adsorption. However, as the pH increases above 5, the functional groups on the DSS adsorbent surface become deprotonated, neutralizing its positive charge. This does not enable additional adsorption of the cationic dye beyond that achieved at pH 5.

Effect of contact time

Fig. 3c shows that MV10B dye adsorption onto the DSS adsorbent was rapid, reaching equilibrium within 30 minutes for all initial dye concentrations tested. The fast adsorption process indicates that the adsorbent is efficient at rapidly capturing dye molecules from solution. This is consistent with previous studies, which have shown that the adsorption of cationic dyes is typically a fast process (Sulyman et al., 2016; Cheruiyot et al., 2019).

Effect of initial concentration

Fig. 3c also shows that the adsorption efficiency increases with increasing initial dye concentration. This is because the number of MV10B dyes ions available for adsorption increases as the initial dye concentration increases, resulting in greater utilization of available adsorption sites on the DSS adsorbent surface.

Several previous studies have reported similar findings regarding the influence of the initial dye concentration on the adsorption efficiency. For example, Lairini et al. (2017) reported that the adsorption capacity of an MV10B dye onto a potato peel adsorbent increased with increasing initial dye concentration (Lairini et al., 2017). Similarly, a study by Loulidi et al. (2020) showed that the adsorption efficiency of an MV10B dye onto an almond shell adsorbent improved with increasing initial dye concentration (Loulidi et al., 2020).

Effect of temperature

Investigating the influence of temperature on dye adsorption is crucial for understanding process dynamics (Agarwala and Mulky, 2023). The findings of this study reveal a decrease in the MV10B dye adsorption efficiency as the temperature increase, which indicates that the MV10B dye adsorption process is not heat dependent. This suggests that the adsorption process can be effectively carried out at ambient or moderate temperatures without the need for additional heating. The decrease in adsorption efficiency with increasing temperature can be attributed to the fact that high temperatures lead to a decrease in the affinity between the adsorbent and the adsorbate and weakening of the interactions on the surface of the adsorbent (Smoczynski, et al., 2020). Similar observations regarding the impact of temperature on adsorption efficiency have been reported in research conducted by Enenebeaku et al. (2016) (Enenebeaku et al., 2016).

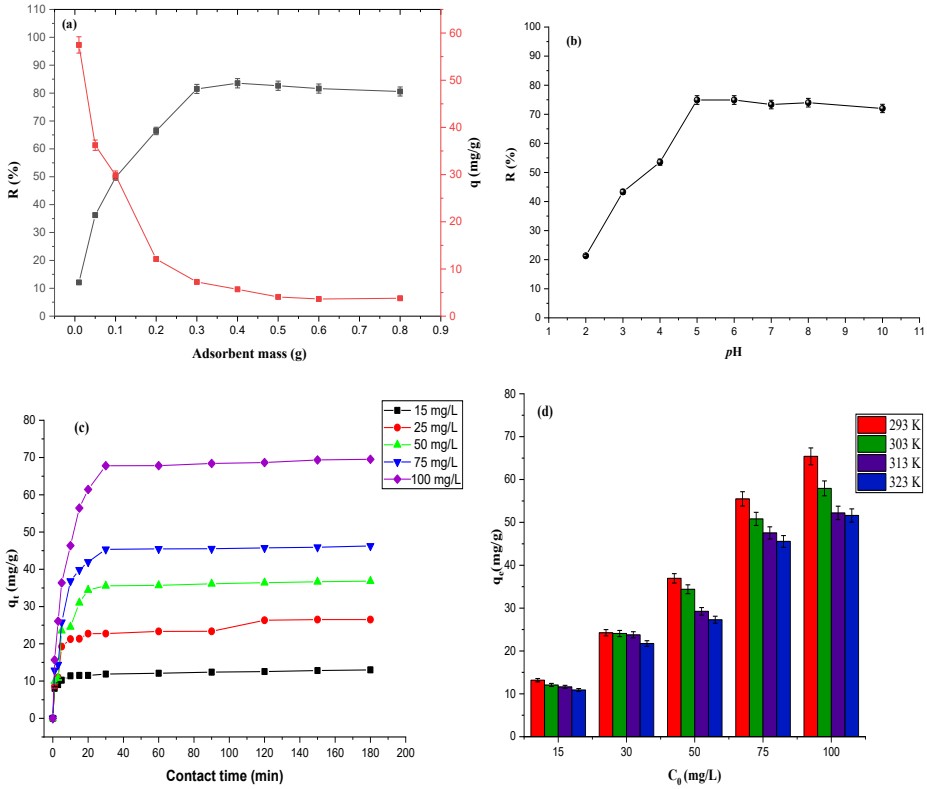

Figure 3: (a) Effect of adsorbent mass; (b) effect of pH; (c) effect of contact time and initial concentration; and (d) effect of temperature on the efficiency of the adsorption of the MV10B dye onto the DSS adsorbent.

Adsorption kinetics

The kinetic analyses of adsorption enable the determination of adsorption rates and diffusion coefficients and elucidate mass transfer resistances (Guffanti et al., 2021).

Kinetic models such as the pseudo first order (PFO), pseudo second order (PSO), Elovich, and Weber-Morris intraparticle diffusion (WMIP) models have proven useful for describing adsorption kinetics. Careful selection of kinetic models based on adsorbent-adsorbate interactions and transport processes is key. Kinetic studies also facilitate comparisons between different adsorbents and the design of adsorption processes for various applications (Benjelloun et al., 2021).

The pseudo-first-order model assumes that adsorption occurs through a single-step process, with the rate-limiting step being the transfer of adsorbate from the bulk solution to the adsorbent surface, and the rate of absorption is proportional to the concentration of the adsorbate (Revellame et al., 2020). The nonlinear equation for the PFO model is represented as Eq. (3):

$$q_t = q_e\left(1 - \mathrm{Exp}\left(-K_1 t\right)\right) \tag{3}$$

Where q_t is the amount of MV10B dye adsorbed at time t (mg/g), q_e is the amount of MV10B dye adsorbed at equilibrium (mg/g), and K_1 is the pseudo-first-order rate constant (1/min).

The pseudo-second-order model postulates that the rate-limiting step is chemisorption and that the adsorption rate is directly proportional to the square of the concentration of unoccupied adsorption sites on the surface (Shukla and Kisku, 2015). The nonlinear equation of the PSO model is expressed as follows:

$$q_t = \frac{q_e^2 K_2 t}{q_e K_2 t + 1} \tag{4}$$

Where q_t is the amount of MV10B dye adsorbed at time t (mg/g), q_e is the amount of MV10B dye adsorbed at equilibrium (mg/g), and K_2 is the pseudo-second-order rate constant (g/(mg·min)).

The Elovich model suggests a multistep adsorption process involving both chemical and physical interactions, and the rate of absorption is proportional to the logarithm of the concentration of the adsorbate (Largitte and Pasquier, 2016), with the nonlinear equation given by Eq. (5):

$$q_t = \frac{1}{\beta}\mathrm{Ln}\left(1 + \alpha\beta t\right) \tag{5}$$

Where q_t is the amount of MV10B dye adsorbed at time t (mg/g) and α and β are the Elovich model constants.

The Weber–Morris intraparticle diffusion model hypothesizes that intraparticle diffusion is one of the rate-determining steps; this model takes into account the rate of diffusion of

the adsorbate into the pores of the adsorbent (Wang and Guo, 2022). The nonlinear equation is represented as Eq. (6):

$$q_t = K_{IP}(t)^{1/2} + C \quad (6)$$

Where q_t is the amount of MV10B dye adsorbed at time t (mg/g) and K_{IP} is the intraparticle diffusion rate constant (mg/(g·min$^{1/2}$)).

In Fig. 4, the nonlinear regressions of the experimental data for the kinetic models are shown, and the calculated parameters are presented in Table 3.

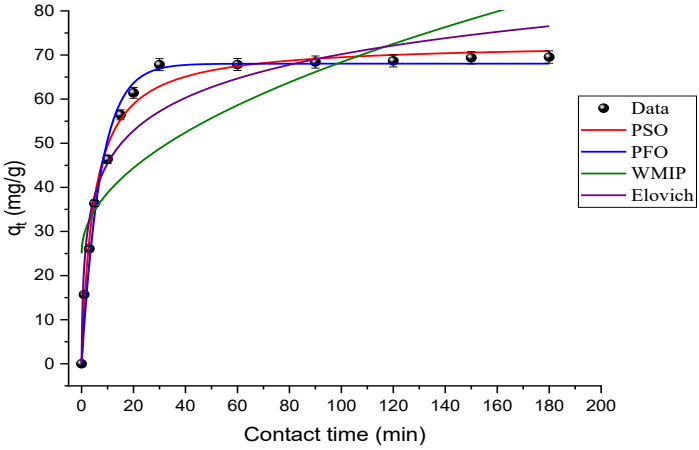

Figure 4: Representations of nonlinear kinetic models for the adsorption of MV10B dye onto DSS.

Table 2: Calculated parameters for nonlinear kinetic models for MV10B dye adsorption onto DSS.

Model	Isotherm parameters	Statistical metrics
Pseudo-first-order	q_e =68.03102+1.22864 K_1=0.13695+0.01096	χ^2= 9.3928 R^2=0.98457 Adj R^2=0.98317
Pseudo-second-order	q_e =72.76808+1.1774 K_2=0.00291+2.83987E-4	χ^2= 5.63598 R^2=0.99074 Adj R^2=0.9899
Elovich	α =71.226+36.779 β=0.0925+0.0107	χ^2= 37.8733 R^2=0.9378 Adj R^2=0.9321
Intraparticle diffusion	C=25.0262+6.5186 K_{IP}=4.3355+0.8986	χ^2= 195.4297 R^2=0.67907 Adj R^2=0.64989

The results obtained in the table 2 indicate that all the statistical metrics, including the coefficient of determination (R^2), adjusted R^2 (Adj R^2), and chi-squared (χ^2) (Jasper et al., 2020), prove that the pseudosecond order kinetic model is the most suitable for this adsorption system, where the pseudosecond order model had the lowest χ^2 value (5.635) compared to the pseudofirst order (9.392), Elovich (37.873) and intraparticle diffusion (195.429) models. In addition, the pseudo-second-order kinetic model had the highest R^2 (0.9907) and Adj R^2 (0.9899) values compared to the pseudo-first-order ($R^2 = 0.9845$, Adj $R^2 = 0.9831$), Elovich ($R^2 = 0.9378$, Adj $R^2 = 0.9321$) and intraparticle diffusion ($R^2 = 0.6790$, Adj $R^2 = 0.6498$) models.

The pseudo-second-order model appropriately describes the change in the MV10B dye adsorption rate over time, with an initially rapid adsorption rate that slows as available DSS adsorbent sites are occupied. By assuming that the adsorption rate is proportional to the square of the MV10B dye surface concentration, this model captures the dynamic nature of the adsorption process as the DSS adsorbent surface becomes saturated. The statistical results validated the pseudo-second-order chemisorption model as the most accurate kinetic model for this MV10B dye-DSS adsorption system.

Adsorption isotherms

To comprehensively elucidate the adsorption mechanism of dyes onto the adsorbent surface and the behavior of the adsorption process, several isothermal models, namely, the Langmuir, Freundlich, and Temkin models, were investigated. These models propose hypotheses regarding the adsorption surface, adsorption layers and their correlation with adsorption conditions. More specifically, the Langmuir model postulates monolayer adsorption on a homogeneous surface with no interaction between adsorbed molecules (Ehiomogue et al., 2022). The Freundlich model describes multilayer adsorption on a heterogeneous surface with a non-uniform distribution of adsorption heat and affinity. The Temkin model suggests that the heat of adsorption of all molecules in the layer decreases linearly rather than logarithmically with surface coverage due to molecular–molecular interactions (Ayawei et al., 2017).

The Langmuir isotherm can be expressed by the following nonlinear form:

$$q_e = q_m \frac{K_L C_e}{1 + K_L C_e} \tag{7}$$

Where q_e is the amount of MV10B dye adsorbed per unit mass of adsorbent at equilibrium, q_m is the maximum amount of dye that can be adsorbed per unit mass of DSS adsorbent, C_e is the equilibrium concentration of MV10B dye in solution, and K_L is the Langmuir constant.

The Freundlich isotherm can be represented by the following nonlinear equation:

$$q_e = K_F C_e^{1/n} \tag{8}$$

Where q_e is the amount of MV10B dye adsorbed per unit mass of DSS adsorbent at equilibrium and K_F and n are the Freundlich constants that must be determined experimentally.

The nonlinear form of the Temkin isotherm can be expressed as follows:

$$q_e = \frac{RT}{b} Ln(K_T C_e) \quad (9)$$

Where q_e is the amount of MV10B dye adsorbed per unit mass of DSS adsorbent at equilibrium, K_T and b are constants that must be determined experimentally, R is the universal gas constant, and T is the temperature.

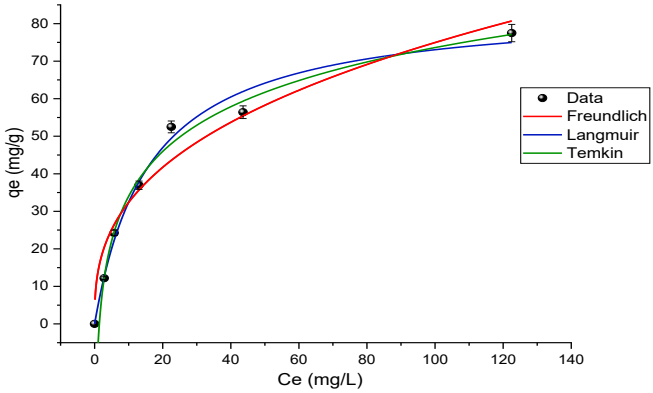

Figure 5: Representations of isotherm models for nonlinear adsorption of MV10B dye onto DSS.

Table 3: Calculated parameters for nonlinear isotherm models for MV10B dye adsorption onto DSS.

Model	Isotherme parameters	Statistical metrics
Langmuir	q_m = 84.83572 ± 4.29053	χ^2= 10.23018
	K_L= 0.06198 ± 0.00925	R^2= 0.98838
		Adj R^2= 0.98606
Freundlich	K_F =14.00686 ± 2.90612	χ^2= 41.40602
	1/n = 0.36427± 0.05166	R^2= 0.94077
		Adj R^2= 0.92596
Temkin	b =17.19795 ± 0.82581	χ^2= 6.37357
	K_T= 0.72302± 0.09779	R^2= 0.99276
		Adj R^2= 0.99131

Fig. 5 shows that the adsorption quantity curve at equilibrium in terms of concentration at equilibrium is of type L according to the Giles et al. (1960) classification.

After analyzing the results of the isotherm models presented in Table 3, it appears that the Temkin model provides the best fit to the experimental data based on the statistical data. Specifically, the lowest χ^2 (6.37357) and R^2 (0.99276) values were closest to 1 compared to those of the other studied models. This suggests that the adsorption system studied exhibits indirect adsorbate-adsorbate interactions on a heterogeneous surface. The positive value of the Temkin constant b (b = 17.19795 > 8 kJ/mol) also indicates that this MV10B dye adsorption process is exothermic (Mabuza et al., 2022). A value of the Freundlich constant 1/n between 0 and 1 further indicates favorable adsorption (Sulyman et al., 2016). However, the maximum adsorption capacity estimated from the Langmuir model was 84.83 mg/g.

Adsorption thermodynamics

To investigate the thermodynamics of the MV10B dye adsorption process and calculate the associated thermodynamic parameters, a Van't Hoff plot was utilized (Lima et al., 2018).

The adsorption data at different temperatures were fitted well to the linear form of the Van't Hoff equation:

$$\mathrm{Ln}\left(\mathrm{K_d}\right) = -\frac{\Delta \mathrm{H}^\circ}{\mathrm{R}} \times \frac{1}{\mathrm{T}} + \frac{\Delta \mathrm{S}^\mathrm{o}}{\mathrm{R}} \tag{10}$$

The changes in enthalpy ($\Delta H°$) and entropy ($\Delta S°$) were determined from the slope and intercept of the linear plot of Ln K versus 1/T, respectively.

The Gibbs free energy change ($\Delta G°$) is related to the equilibrium constant (K_d) of MV10B dye adsorption through the following equation:

$$\Delta \mathrm{G}^\circ = -\mathrm{RT} \times \mathrm{Ln}(\mathrm{K_d}) \tag{11}$$

$$\mathrm{K_d} = \mathrm{q_e}/\mathrm{C_e} \tag{12}$$

Where K_d is the equilibrium constant of MV10B dye adsorption, T is the absolute temperature (K), and R is the universal gas constant (8.314 J/mol K).

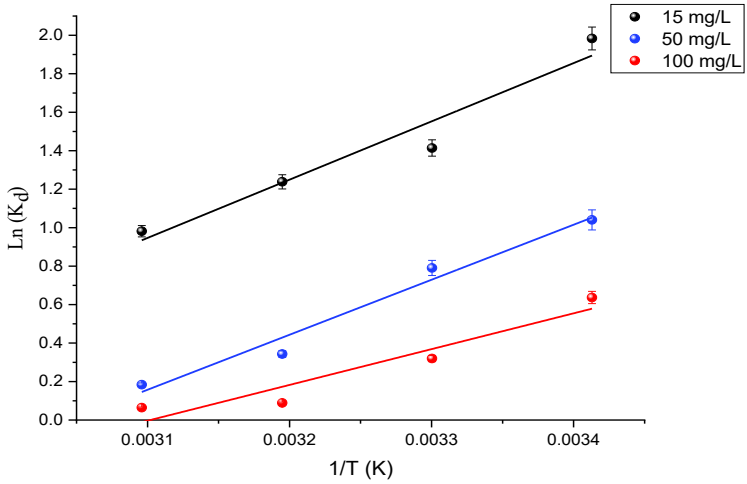

Figure 6: Plot of ln (Kd) vs 1/T for MV10B dye adsorption onto DSS

Table 4: Thermodynamic parameters for MV10B dye adsorption onto DSS

C_0 [mg/L]	T [K]	ΔG° [kJ/mol]	ΔH° [kJ/mol]	ΔS° [J/(mol K)]	RSS	R^2	r
15	293	-4.8315	-25.185	-70.205	0.0295	0.9455	0.9724
	303	-3.4444					
	313	-3.0162					
	323	-2.3901					
50	293	-2.5343	-23.775	-72.394	0.0125	0.9733	0.9865
	303	-1.9252					
	313	-0.8354					
	323	-0.4470					
100	293	-1.5517	-15.472	- 47.994	0.0186	0.9121	0.9550
	303	-0.7791					
	313	-0.2160					
	323	-0.1570					

The thermodynamic parameters of the MV10B dye adsorption process were calculated using the Van't Hoff plot graph presented in Fig. 6, and these results are compiled in Table 4. The negative values of the Gibbs free energy ($-4.83<\Delta G°<0$ kJ/mol) indicate that this adsorption process occurred spontaneously, signifying a favorable and energetically feasible process (Yunusa and Ibrahim, 2020). Moreover, the negative values of enthalpy ($-25.18<\Delta H°<0$ kJ/mol) and entropy ($-72.39<\Delta S°<0$ J/mol K) suggest that the MV10B dye adsorption process is exothermic and leads to a decrease in randomness during this adsorption (Jia et al., 2018). Additionally, to evaluate the goodness of fit between the

experimental data and the Van't Hoff plot, several statistical criteria were employed, including the coefficient of determination (R^2), residual sum of squares (RSS), and Pearson's correlation coefficient (r). The high values of R^2 (0.91-0.94) and Pearson's r (0.95-0.98), along with the low RSS values (0.012-0.029), demonstrate strong agreement between the experimental data and the model provided by the Van't Hoff plot. This demonstrates the suitability of the Van't Hoff plot for the investigated MV10B dye adsorption process.

MV10B dye adsorption mechanism

The precise determination of the adsorption mechanism is a complex process, as various factors contribute to understanding how adsorption occurs. Key aspects include the nature of the adsorbent surface and the dye charge (Loulidi et al., 2020). The FTIR analysis revealed the presence of essential functional groups such as hydroxyl and carboxyl in the cellulose, hemicellulose, and lignin components of the DSS adsorbent. These functional groups play an important role in adsorption by forming interactions like hydrogen bonds, Van der Waals or electrostatic interactions or and reducing π-π dispersion interactions between the aromatic rings of the dyes and the adsorbent surface (Qiu et al., 2009). Furthermore, rapid adsorption kinetics and thermodynamic investigations have shown that the MV10B dye adsorption process is exothermic, with an absolute enthalpy value between 20 and 80 kJ/mol, indicating a physisorption process. This finding supports the significant contribution of electrostatic interactions to the MV10B dye adsorption process (Loulidi et al., 2020; Cheruiyot et al., 2019).

Comparative Assessment

Table 5 represents the assessment of various raw adsorbents for their monolayer capacity in removing Methyl Violet 10B Dye under optimum conditions.

Table 5: Methyl Violet 10B dye removal efficiency of different raw adsorbents

Adsorbents	Monolayer capacity [mg/g]	References
Almond leaves powder	22.96	(Okorocha et al., 2016)
Almond Shell	114	(Ishaq et al., 2016)
Cedar Cone Forest	13.64	(Zamouche et al., 2020)
Salix alba L. Forest	35.21	(Gemici et al., 2023)
Salix babylonica L. Forest	36.50	(Gemici et al., 2023)
Red seaweed	5.714	(Al-Saeedi et al., 2023)
Dry Spearmint Sprigs	84.83	Present study

The results presented in the table 5, which displays the maximum adsorption values for some various raw adsorbents, indicate that the Dry Spearmint Sprigs adsorbent used in this study yielded competitive results and was found to be satisfactory. This suggests that this Dry Spearmint Sprigs is a promising candidate for future applications in water treatment, given its ability to effectively remove Methyl Violet 10B dye.

CONCLUSION

This research makes substantial contributions to the fields of environmental protection, human and animal health, and sustainable industrial practices. This study provides essential insights into effective strategies for mitigating the adverse impacts of synthetic aquatic dyes on ecosystems.

The investigation successfully determined the optimal conditions for the process of adsorbing MV10B dye onto DSS, where a DSS adsorbent mass of 0.01 g, a pH of 5, and an equilibration time of 30 minutes demonstrated the most favorable outcomes. The adsorption capacity exhibited a positive correlation with the initial MV10B dye concentration but was inversely related to temperature.

Statistical analyses favored the pseudo-second-order kinetic model, followed by the first-order pseudo model, Elovich model, and intraparticle diffusion model.

Regarding the isothermal models, the Temkin isotherm exhibited the best fit, with the Langmuir and Freundlich isotherms also displaying good suitability. The maximum adsorption capacity for monolayer adsorption was 84.83 mg/g.

Thermodynamic analysis indicated negative values for $\Delta G°$ ($-4.83<\Delta G°<0$ kJ/mol), $\Delta H°$ ($-25.18<\Delta H°<0$ kJ/mol), and $\Delta S°$ ($-72.39<\Delta S°<0$ J/mol K), confirming the spontaneous, exothermic, and less random nature of the MV10B dye adsorption process.

Declaration of competing interest

The authors declare that they have no known competing financial interests or personal relationships that could have appeared to influence the work reported in this paper.

REFERENCES

ABBA P., PENGOU M., BALKISSOU S., BADJOUKOUN Y., DELSIA L.J., DANGA R., ABDOUL W. (2019). Removal of purple of bromocresol from aqueous solutions by biosorption on a tropical biomass: the triplochiton scleroxylon (ayus) saw, Larhyss Journal, No.39, pp. 59–76.

ADAK A., BANDYOPADHYAY M., PAL A. (2005). Removal of crystal violet dye from wastewater by surfactant-modified alumina. Separation and Purification Technology, Vol. 44, pp. 139–144, doi: 10.1016/j.seppur.2005.01.002.

ADAPA P. K., TABIL L. G., SCHOENAU G. J., CANAM T., DUMONCEAUX T. (2011). Quantitative Analysis of Lignocellulosic Components of Non-Treated and Steam Exploded Barley, Canola , Oat and Wheat Straw Using Fourier Transform Infrared Spectroscopy. Journal of Agricultural Science and Technology, Vol. B1 pp. 177–188.

ADESANM B.M., PAUL H., HUHNKE C., ADESANMI B.M., HUNG Y., PAUL, H.H., HUHNKE C.R. (2022). EngagedScholarship @CSU Civil and Environmental Engineering Faculty Comparison of dye wastewater treatment methods : A review . Comparison of dye wastewater treatment methods : A review. GSC Advanced Research and Reviews, Vol. 10, pp. 126–137.

AGARWALA R., MULKY L. (2023). Adsorption of Dyes from Wastewater : A Comprehensive Review, ChemBioEng Reviews, Vol. 10, No. 3, pp. 326–335, doi: 10.1002/cben.202200011.

AL-SAEEDI S.I., ASHOUR M., ALPROL A.E. (2023). Adsorption of toxic dye using red seaweeds from synthetic aqueous solution and its application to industrial wastewater effluents, Frontiers in Marine Science, Vol. 10, No August, pp. 1–20, doi: 10.3389/fmars.2023.1202362.

AL-SHAMMARI, N.H., AL-MAMMAR, D.E. (2022). Equilibrium and kinetic modeling studies for the adsorption-desorption of methyl violet 10B onto leather waste, Eurasian Chemical Communications, Vol. 4, No 2, pp. 175–189, doi: 10.22034/ecc.2022.317547.1274.

AL-TOHAMY R., ALI S.S., LI F., OKASHA K.M., MAHMOUD Y.A., ELSAMAHY T., JIAO H., et al. (2022). Ecotoxicology and Environmental Safety A critical review on the treatment of dye-containing wastewater : Ecotoxicological and health concerns of textile dyes and possible remediation approaches for environmental safety, Ecotoxicology and Environmental Safety, Elsevier Inc., Vol. 231, p. 113160, doi: 10.1016/j.ecoenv.2021.113160.

AROUA-BERKAT S., AROUA N. (2022), Opportunities and Challenges for Wastewater Reuse in Algeria, Larhyss Journal, No. 51, pp. 7–17.

AYAWEI N., EBELEGI A.N., WANKASI D. (2017). Modelling and Interpretation of Adsorption Isotherms, Journal of Chemistry, Article ID 3039817, doi: 10.1155/2017/3039817.

BELHOUALA K., BENARBA B. (2021). Medicinal Plants Used by Traditional Healers in Algeria: A Multiregional Ethnobotanical Study, Frontiers in Pharmacology, Vol. 12, pp. 1–23, doi: 10.3389/fphar.2021.760492.

BENJELLOUN M., MIYAH Y., AKDEMIR G., ZERROUQ F., LAIRINI S. (2021). Recent Advances in Adsorption Kinetic Models : Their Application to Dye Types, Arabian Journal of Chemistry, Vol. 14, No. 4, Paper 103031. doi: 10.1016/j.arabjc.2021.103031.

BENSLAMA H. BOUKET A.C., POURHASSAN Z., ALENEZI F.N., SILINI A. (2021). Diversity of Synthetic Dyes from Textile Industries, Discharge Impacts and Treatment Methods, Applied Sciences, Vol. 11, No. 14, pp. 1–21.

BERRADI M., HSISSOU R., KHUDHAIR M., ASSOUAG M., CHERKAOUI O., EL BACHIRI A., EL HARFI A. (2019). Textile finishing dyes and their impact on aquatic environs, Heliyon, Vol. 5, No. 11, doi: 10.1016/j.heliyon.2019.e02711.

CASTELLAR-ORTEGA G.C., CARDOZO-ARRIETA B.M., JARAMILLO-COLPAS J.E., MORENO-ALDANA L.C. (2022). Journal of Applied Research and Technology, Vol. 20, pp. 387–398.

CHAUHAN S.S., DIKSHIT P.K.S. (2023). Cadmium Metal Scavenging Capability of Spent Tea Grains-an Agricultural Biomass Waste As a Low-Cost Adsorbent, Larhyss Journal, No. 55, pp. 161–189.

CHERUIYOT G.K., WANYONYI W.C., KIPLIMO J.J., MAINA E.N. (2019). Adsorption of toxic crystal violet dye using coffee husks : Equilibrium , kinetics and thermodynamics study, Scientific African, Vol. 5, pp. 1–11.

doi: 10.1016/j.sciaf.2019.e00116.

DENG Z., XIA A., LIAO Q., ZHU X., HUANG Y., FU Q. (2019). Biotechnology for Biofuels Laccase pretreatment of wheat straw : effects of the physicochemical characteristics and the kinetics of enzymatic hydrolysis, Biotechnology for Biofuels, BioMed Central, Vol.12, pp. 1–13, doi: 10.1186/s13068-019-1499-3.

DJEHAF K., BOUYA A.Z., OUHIB R., BENMANSOUR H., BENTOUAF A., MAHDAD A., MOULAY N. (2019). Textile wastewater in Tlemcen (Western Algeria): Impact, treatment by combined process, Chemistry International, Vol. 3, No. 4, pp. 314–319.

DOCAMPO R., MORENO S.N. (1990). The metabolism and mode of action of gentian violet, Drug Metabolism Reviews, Vol. 22, Issues 2-3, pp. 161–178.

EHIOMOGUE P., AHUCHAOGU I.I., AHANEKU I.E. (2022). Review of adsorption isotherms models, Acta Technica Corviniensis, Vol. 14, No. 4, pp. 87–96.

EL NAEEM, G.A., ABD-ELHAMID A.I., FARAHAT O.O.M., EL-BARDAN A.A., SOLIMAN H.M.A., NAYL, A.A. (2022). Adsorption of crystal violet and methylene blue dyes using a cellulose-based adsorbent from sugercane bagasse : characterization , kinetic and isotherm studies, Journal of Materials Research and Technology, Vol. 19, pp. 3241–3254, doi: 10.1016/j.jmrt.2022.06.045.

ENENEBEAKU C.K., OKOROCHA N.J., ENENEBEAKU U.E., ONYEACHU, B.I. (2016). Removal of Crystal Violet Dye by Adsorption onto Picrilima Nitida Stem Bark Powder : Kinetics and Isotherm Studies, IOSR Journal of Applied Chemistry, Vol. 9, No. 8, pp. 14–23, doi: 10.9790/5736-0908011423.

GEMICI B.T., OZEL H.U., OZEL H.B. (2023). Adsorption property and mechanism of forest wastes based naturel adsorbent for removal of dye from aqueous media, Biomass Conversion and Biorefinery, Vol. 13, pp. 13653–13665.

GUFFANTI S., VISCONTI C.G., GROPPI G. (2021). Model Analysis of the Role of Kinetics , Adsorption Capacity , and Heat and Mass Transfer Effects in Sorption Enhanced Dimethyl Ether Synthesis, Vol. 60, No. 18, pp. 6767-6783, doi: 10.1021/acs.iecr.1c00521.

HAMZA H., MOKRANI D., NIA B., TOUIL A. (2022). Use of traditional medicine in Algeria as an alternative treatment against COVID-19 in the context of modern medicine: a survey-based study, Infectious Diseases Research, Vol. 3, No. 2, p. 7, doi: 10.53388/idr20220525007.

IMRAN M.S., JAVED T., AREEJ I., HAIDER N.M.,(2022). Sequestration of crystal violet dye from wastewater using low-cost coconut husk as a potential adsorbent, Water Science & Technology, Vol. 85, No. 8, pp. 2295–2317. doi: 10.2166/wst.2022.124.

ISHAQ M., JAVED F., AMAD I., ULLAH H., HADI F., SULTAN S. (2016). Adsorption of Crystal Violet dye from aqueous solutions onto low-cost untreated and NaOH treated almond shell, Iranian Journal of Chemistry and Chemical Engineering, Vol. 35, No. 2, pp. 97–106.

JASPER E.E., AJIBOLA V.O., ONWUKA J.C. (2020). Nonlinear regression analysis of the sorption of crystal violet and methylene blue from aqueous solutions onto an agro-waste derived activated carbon, Applied Water Science, Vol. 10, No. 6, pp. 1–11, doi: 10.1007/s13201-020-01218-y.

JIA P., TAN H., LIU K., GAO W. (2018). Applied sciences Removal of Methylene Blue from Aqueous Solution by Bone Char, Applied Sciences, Vol. 8, No. 10, Paper 1903, doi: 10.3390/app8101903.

JOHN A., YANG H., MUHAMMAD S., KHAN Z.I., YU H., LUQMAN M., TOFAIL M., et al. (2022). Applied sciences Cross Talk between Synthetic Food Colors (Azo Dyes), Oral Flora , and Cardiovascular Disorders, Applied Sciences, Vol. 12, No. 14, Paper 7084, doi:10.3390/app12147084

KANT A., GAIJON P., NADEEM U. (2014). Adsorption Equilibrium and Kinetics of Crystal Violet Dye from Aqueous Media onto Waste Material, Chemical Science Review and Letters, Vol. 3, No.11S, pp. 1–13.

KHELIFI O., MEHREZ I., YOUNSI M., NACEF M., AFFOUNE A.M. (2018). Methyl orange adsorption on biosorbent derived from Mango seed kernels, Larhyss Journal, No. 36, pp. 145–156. (In French)

KHELIFI O., MEHREZ I., BEN SALAH W., BEN SALAH F., YOUNSI M., NACEF M., AFFOUNE A.M. (2016). Study of methylene blue (MB) adsorption from aqueous solutions on biosorbent prepared from Algerian datte stones, Larhyss Journal, No 28, pp. 135-148. (In French)

KHELILI H., ACHOUR S., KONAN K.G., GUELLAL M. (2024). Kinetic and isotherm study of Methylene blue adsorption on orange peel activated carbon, Larhyss Journal, No 58, pp. 89-103.

KYI P.P., QUANSAH J.O., LEE C.G., MOON J.K., PARK S.J. (2020). The Removal of Crystal Violet from Textile Wastewater Using Palm Kernel Shell-Derived Biochar, Applied Sciences, Vol. 10, No. 7, Paper 2251.

LAIRINI S., EL MAHTAL K., MIYAH,Y., TANJI,K., GUISSI S., BOUMCHITA S., ZERROUQ F. (2017). The adsorption of Crystal violet from aqueous solution by using potato peels (*Solanum tuberosum*): Equilibrium and kinetic studies, Journal of Materials and Environmental Science, Vol. 8, No. 9, pp. 3252–3261.

LARGITTE L., PASQUIER R. (2016). Chemical Engineering Research and Design A review of the kinetics adsorption models and their application to the adsorption of lead by an activated carbon, Chemical Engineering Research and Design, Institution of Chemical Engineers, Vol. 109, pp. 495–504, doi: 10.1016/j.cherd.2016.02.006.

LIMA E.C., BANDEGHARAEI A.H., PIRAJAN J.C.M. (2018). A critical review of the estimation of the thermodynamic parameters on adsorption equilibria. Wrong use of equilibrium constant in the Van't Hoof equation for calculation of thermodynamic parameters of adsorption, Journal of Molecular Liquids, Vol. 273, pp. 425–434, doi: 10.1016/j.molliq.2018.10.048.

LOULIDI I., BOUKHLIFI F., OUCHABI M., AMAR A., JABRI M., KALI A., CHRAIBI S., et al. (2020). Adsorption of Crystal Violet onto an Agricultural Waste Residue : Kinetics , Isotherm , Thermodynamics , and Mechanism of Adsorption, Hindawi, Vol. 2020. Article ID 5873521, doi:10.1155/2020/5873521

MABUZA M., PREMLALL K., DARAMOLA M.O. (2022). Modelling and thermodynamic properties of pure CO_2 and flue gas sorption data on South African coals using Langmuir, Freundlich, Temkin, and extended Langmuir isotherm models, International Journal of Coal Science and Technology, Springer Nature Singapore, Vol. 9, No. 1, doi: 10.1007/s40789-022-00515-y.

MAHMOOD H., MAHMOOD F. (2023). Ficus Benjamin's leaf, a native sorbent for the exclusion of Methyl violet 10B from aquatic media, Heliyon, Vol. 9, No. 3, Paper e14295, doi: 10.1016/j.heliyon.2023.e14295.

MANI S., BHARAGAVA R.N. (2016). Exposure to Crystal Violet , Its Toxic , Genotoxic and Carcinogenic Effects on Environment and Its Degradation and Detoxification for Environmental Safety, Reviews of Environmental Contamination and Toxicology, Vol. 237, pp. 71-104, doi: 10.1007/978-3-319-23573-8.

MESSAOUD-BOUREGHDA M.Z., AKSAS H., LOUHAB K., (2013). The study of potable water treatment process in Algeria (Boudouaou station) -by the application of life cycle assessment (LCA), Journal of Environmental Health Science & Engineering, pp. 1–9.

MRE (Algerian Ministry of Water Resources) (2022). The volume of treated wastewater is estimated at 500 million m^3/year, Algeria Press Service, https://www.aps.dz/economie/136888-le-volume-des-eaux-usees-epurees-estime-a-500-millions-m3-an, 10 March 2022. (In French)

OKOROCHA N.J., OKOJI J.J., OSUJI C. (2016). Adsorption of Basic and Acidic Dyes onto Agricultural Wastes, International Letters of Chemistry, Physics and Astronomy, Vol. 70, pp. 12–26, doi: 10.56431/p-7cw7it.

OUETTAR L.,GUECHI E.,OUALID HAMDAOUI O., FERTIKH N., SAOUDI F., ABUDULAZIZ ALGHYAMAH A. (2023). Biosorption of Triphenyl Methane Dyes (Malachite Green and Crystal Violet) from Aqueous Media by Alfa (Stipa tenacissima L.) Leaf Powder, Molecules, Vol. 28, No. 8, Paper ID 3313.

OUAKOUAK A.K., YOUCEF L. (2016). Adsorption of Cu2+ ions on powder activated carbon and a sodique bentonite, Larhyss Journal, No 27, pp. 39-61. (In French)

PENNINKS A., BAERT K., LEVORATO S., BINAGLIA M. (2017). Dyes in aquaculture and reference points for action, European Food Safety Authority (EFSA), Vol. 15, doi: 10.2903/j.efsa.2017.4920.

PANDEY K.K., PITMAN A.J. (2003). FTIR studies of the changes in wood chemistry following decay by brown-rot and white-rot fungi, International Biodeterioration & Biodegradation, Vol. 52, No.3, pp. 151–160, doi: 10.1016/S0964-8305(03)00052-0.

PETKOVA I.L., KIRILOVA D.A., STOYANOVA V.P. (2019). Characterization of Two Bulgarian Herbs for Use as Biosorbents for Copper (II) Characterization of Two Bulgarian Herbs for Use as Biosorbents for Copper (II) Lidia Petkova Ivanova, Albena Kirilova Detcheva & Paunka Stoyanova, Analytical Letters, Vol. 0 No. 0, pp. 1–13, doi: 10.1080/00032719.2019.1587447.

PRIYANTHA N., ROMZI A.A., CHAN C.M., LIM L.B.L. (2021). Enhancing adsorption of crystal violet dye through simple base modification of leaf adsorbent: Isotherm, kinetics, and regeneration, Desalination and Water Treatment, Vol. 215, pp. 194–208, doi: 10.5004/dwt.2021.26758.

QIU Y., ZHENG Z., ZHOU Z., SHENG G.D. (2009), Effectiveness and mechanisms of dye adsorption on a straw-based biochar, Bioresource Technology, Elsevier Ltd, Vol. 100, No. 21, pp. 5348–5351, doi: 10.1016/j.biortech.2009.05.054.

REHMAN F., SAYED M., KHAN J.A.L.I., KHAN H.M. (2017). Removal of crystal violet dye from aqueous solution by gamma irradiation, Journal of the Chilean Chemical Society, Vol.62, No.1, pp. 3359–3364.

REN S., GUO J., ZENG G., SUN, G. (2006). Decolorization of triphenylmethane, azo, and anthraquinone dyes by a newly isolated Aeromonas hydrophila strain, Appl Microbiol Biotechnol, Vol.72, No.6, pp. 1316–1321, doi: 10.1007/S00253-006-0418-2.

REVELLAME E.D., LORD D., SHARP W., HERNANDEZ R., ZAPPI M.E. (2020). Adsorption kinetic modeling using pseudo first order and pseudosecond order rate laws : A review, Cleaner Engineering and Technology, Vol. 1, Paper 100032, doi: 10.1016/j.clet.2020.100032.

REZAZADEH M., BAGHDADI M., MEHRDADI N., ABDOLI M.A. (2021). Adsorption of crystal violet dye by agricultural rice bran waste: Isotherms, kinetics, modeling and influencing factors, Environmental Engineering Research, Vol. 26, No. 3, pp. 0–2, doi: 10.4491/eer.2020.128.

SAMAI I., NEBBACHE S., AOUNALLAH O., RAMDANI H. MEGHLAOUI Z. (2023). Water pollution of the Oued D'Hous River (Algeria) and its potential impact on fauna and flora, Journal of Animal Behaviour and Biometeorology, Vol. 11, No. 1, pp. 1–9, doi: 10.31893/jabb.23006.

SHUKLA S.P., KISKU G.C. (2015). Linear and Non-Linear Kinetic Modeling for Adsorption of Disperse Dye in Batch Process, Research Journal of Environmental Toxicology, Vol. 9, No. 6, pp. 320–331, doi: 10.3923/rjet.2015.320.331.

SOLTANI A.,FARAMARZI M., ABOUTALEB S., PARSA M., (2021). A review on adsorbent parameters for removal of dye products from industrial wastewater", Water Quality Research Journal, Vol. 56, No. 4, pp. 181–193. doi: 10.2166/wqrj.2021.023.

SMOCZYNSKI L. PIEROZYNSKI B., MIKOŁAJCZYK T. (2020). Processes The Effect of Temperature on the Biosorption of Dyes, Processes, Vol. 8, No. 6, Paper 636, doi:10.3390/pr8060636

SULYMAN, M., NAMIEŚNIK, J., GIERAK, A. (2016). Adsorptive Removal of Aqueous Phase Crystal Violet Dye by Low-Cost Activated Carbon Obtained from Date Palm (L .) Dead Leaflets, Engineering and Protection of Environment, Vol. 19 No. 4, pp. 611–631, doi: 10.17512/ios.2016.4.14.

SUN M., RICKER K., OSBORNE G. (2019). Evidence on the Carcinogenicity of Gentian Violet, Reproductive and Cancer Hazard Assessment Branch Office of Environmental Health Hazard Assessment California Environmental Protection Agency, No. January, Paper 117.

SRINIVAS C.V.S., ABHISHAY A.D., KUSUMA A., GOWTHAMI Y. (2023). Optimization, kinetics and thermodynamics for the removal of crystal violet dye using synthesized FeNPs from Carica papaya leaves extract, Materials Today: Proceedings, doi: 10.1016/j.matpr.2023.04.035.

YEDDOU MEZENNER N., BENSAADI Z., LAGHA H. BENSMAILI A. (2012). Study of the adsorption of a mixture of biorecalcitrant compounds in an aqueous medium, Larhyss Journal, No 11, pp. 7-16. (In French)

YOUCEF L., OUAKOUAK A., BOULANOUAR D., ACHOUR S. (2014). Study of the adsorbent power of powdered activated carbon for the elimination of phosphates from natural waters, Larhyss Journal, No 17, pp. 35-46. (In French)

YUNUSA U., IBRAHIM M.B. (2020). Adsorptive Removal of Basic Dyes and Hexavalent Chromium from Synthetic Industrial Effluent : Adsorbent Screening , Kinetic and Thermodynamic Studies, I. J. Engineering and Manufacturing, Vol. 5 No. August, pp. 54–74, doi: 10.5815/ijem.2020.04.05.

ZAMOUCHE M., HABIB A., SAAIDIA K., BENCHEIKH L.M. (2020). Batch mode for adsorption of crystal violet by cedar cone forest waste, SN Applied Sciences, Springer International Publishing, Vol. 2, No. 2, pp. 1–9, doi: 10.1007/s42452-020-1976-0.

WANG J., GUO X.G. (2022). Rethinking of the intraparticle diffusion adsorption kinetics model_ Interpretation, solving methods and applications - ScienceDirect, Chemosphere, Vol. 309, ID. 136732. doi: 10.1016/j.chemosphere.2022.136732.